

Growth of magnesium aluminate nanocrystallites

Cite this: *CrystEngComm*, 2014, 16, 1579Dayong Tan,^{ab} Wei Zhou,^b Wenzhu Ouyang,^c Zhongying Mi,^a Lingping Kong,^a Wansheng Xiao,^b Kai Zhu^b and Bin Chen^{*a}Received 27th August 2013,
Accepted 11th November 2013

DOI: 10.1039/c3ce41718b

www.rsc.org/crystengcomm

Nanocrystalline magnesium aluminate was synthesized with the coprecipitation method. Its growing behaviors as a function of temperature were studied with synchrotron X-ray diffraction (XRD) and Raman spectroscopy. It is found that the particle growth was greatly inhibited at temperatures below 1000 °C due to the hydroxide precursor reactants. Above 1000 °C, magnesium aluminate nanoparticles start to grow fast. After two hours annealing at 1200 °C, the grain size changes by multiple folds, suggesting that oriented attachment may occur. Above 1200 °C, the grain size changes in various directions are much smaller than the average grain size, indicating the oriented attachment mechanisms become inactive in the growth of MgAl₂O₄ nanoparticles with sizes larger than 42 nm.

Introduction

Understanding the mechanisms of crystal growth is important for materials science, chemistry, mineralogy and nano-scale science. The knowledge of growing mechanisms is very useful for improving synthesis methods and controlling crystal structures, morphology and particle size. Classically, crystal growth has been described in terms of growth of large particles at the expense of smaller particles, driven by surface energy reduction (Ostwald ripening). About ten years ago, Penn and Banfield discovered another growth mechanism, oriented attachment of crystallites.¹ Both diffusion and oriented attachment mechanisms have been intensively investigated for the growth of nanocrystallites in recent years.^{2–5} However, as far as we know, no oriented attachment has been reported for crystal growth *via* calcinations. In this study, we examine the growing behaviors of nanocrystalline MgAl₂O₄ after calcinations at various temperatures for investigating the crystal growth mechanisms that possibly involve oriented attachment.

Spinel represents one of the most important structure groups in ceramics. Its rheological properties have a wide range of implications from materials science to earth sciences. We choose the archetypal end-member MgAl₂O₄ spinel mainly because its normal, ordered spinel structure is stable over a wide temperature and pressure range and the lack of pre-phase-transition disordering allows us to focus on

the thermally-induced crystallite growth. MgAl₂O₄ spinel has a high melting point (2135 °C), high resistance against chemical attack, good mechanical strength, low dielectric constant, and excellent optical properties, and therefore has wide applications. For instance, (1) MgAl₂O₄ is usable as an infrared radiation lens and as an impact resistant optical window for missile domes.^{6,7} (2) MgAl₂O₄ shows high resistance to most acids and alkalis and has low electrical losses, and thus has a wide range of applications in structural, chemical, optical and electrical industries.^{8,9} It is used as a refractory in linings of steel-making furnaces, transition and burning zones of cement rotary kilns, checker work of the glass furnace regenerators, sidewalls and bottom of the steel ladles, glass furnaces and melting tanks, and as a dense coating for chemical reactors. (3) MgAl₂O₄ spinel occurs as an accessory mineral in basic igneous rocks, in aluminum-rich metamorphic rocks, and in contact-metamorphosed limestones.^{10–12}

It is well known that the stability, behaviors and properties of nanocrystallite materials are critically dependent upon their initial size and morphology. Various synthesis methods of MgAl₂O₄ nanoparticles have been developed and improved. These methods include sol-gel,^{13,14} combustion,^{15–17} hydrothermal,^{18,19} Pechini,^{20–22} coprecipitation,^{23–25} flame spray pyrolysis²⁶ and freeze-drying.²⁷ Recently, a comparative investigation on the synthesis and sintering behavior of MgAl₂O₄ spinel nanoparticles has been carried out between polymeric precursor (Pechini) and coprecipitation methods.²⁸ The authors evaluated the characterization of nanocrystallites synthesized with both methods in their purity and surface cleanliness, size distribution, state of agglomeration, and sintering behavior. Their work provided useful guidance in the synthesis of ultrafine nanoparticles. By tracking the grain size changes after sintering, we hope to gain more insight on the crystallite growing mechanisms.

^a Center for High Pressure Science and Technology Advanced Research, 1690 Cailun Rd, Pudong, Shanghai 201203, PR China. E-mail: chenbin@hpstar.ac.cn

^b Key Laboratory of Mineralogy and Metallogeny, Guangzhou Institute of Geochemistry, Chinese Academy of Sciences, Guangzhou 510640, Guangzhou, PR China

^c Department of Physics and Chemistry, Bozhou Teachers College, Anhui 236800, Bozhou, PR China

Experimental

The hydroxide precursor of MgAl_2O_4 was synthesized *via* the coprecipitation method.²⁸ 1:2 molar ratio stoichiometric amounts of magnesium nitrate [$\text{Mg}(\text{NO}_3)_2 \cdot 6\text{H}_2\text{O}$, 98%] and aluminum nitrate [$\text{Al}(\text{NO}_3)_3 \cdot 9\text{H}_2\text{O}$, 98%] were dissolved in distilled water under magnetic stirring, forming a homogeneous solution. The solution was dripped into a 1 M ammonia solution. The mixed solution was stirred rapidly while there was enough excess ammonia so that the pH fluctuations throughout the process could be neglected. The mixed solution became opaque and a white slurry formed that was then vacuum filtered through a filter paper. The resulted white precipitate was washed with distilled water. The washed precipitate was dried for 24 hours in air at 100 °C. The dried precipitate was ground in a quartz mortar. The resulted samples were divided into seven portions. Each portion was calcined in air at various temperatures with a heating rate of 10 °C min^{-1} . The detailed calcination information of the seven portions is listed in Table 1.

X-ray diffraction measurements were made on the postcalcined coprecipitation powders at the BL15U1 beamline of the Shanghai Synchrotron Radiation Facility (SSRF). A Mar-165 CCD was used to collect the diffraction patterns. The wavelength of the monochromatic X-ray beam was 0.6199 Å. Based on calibration using a standard material, CeO_2 , the distance between the sample and the detector was 179.23 mm. The crystal grain size was estimated according to the Scherrer equation $D = K\lambda/(\beta\cos\theta)$, where K is a dimensionless constant ($K = 0.94$), λ the wavelength of incident X-rays, and β the full width at half maximum of the diffraction peak. 2θ is the diffraction angle. Although the Scherrer size is biased toward larger particles because it measures the volume rather than surface area weighted average, the TEM *versus* XRD results of Gribb and Banfield showed that the Scherrer size can be effectively used to study particle size evolution, especially when the size distribution is fairly tight and the particle size is small.²⁹

Micro-Raman spectroscopy was measured with an inVia Renishaw spectrometer. A solid laser with the wavelength of 532.4 nm was irradiated to the samples. The size of the laser beam was 1–2 μm . Rayleigh scattering light was cut by a Rayleigh filter. Raman spectra were detected by a standard CCD array detector. The exposure time for a spectrum is 30 seconds. The wavenumbers of the Raman shifts were calibrated using single crystalline silicon.

Table 1 Seven batch samples were sintered at various temperatures, e.g. the sample of batch 5 was sintered for 12 hours at 600 °C, 700 °C, 800 °C, and 900 °C, respectively, with another 2 hours at 1000 °C

	600 °C	700 °C	800 °C	900 °C	1000 °C	1200 °C	1400 °C
Batch 1	12 h						
Batch 2	12 h	12 h					
Batch 3	12 h	12 h	12 h				
Batch 4	12 h	12 h	12 h	12 h			
Batch 5	12 h	12 h	12 h	12 h	2 h		
Batch 6	12 h	12 h	12 h	12 h	2 h	2 h	
Batch 7	12 h	12 h	12 h	12 h	2 h	2 h	2 h

Results and discussion

The sample powders were calcined at 600, 700, 800, 900, 1000, 1200 and 1400 °C. The postcalcined coprecipitated powders were white in color. Fig. 1 shows the X-ray diffraction patterns of the samples annealed at different temperatures. The spinel phase was observed at temperatures as low as 600 °C. All the diffraction peaks can be indexed to the spinel crystalline structure (JCPDS card, no. 21-1152). Fig. 2 shows the Raman spectra of the samples after calcinations. On basis of the irreducible representation of the vibration mode symmetry with space group $Fd\bar{3}m$, $\Gamma = A_{1g} + E_g + F_{1g} + 3F_{2g} + 4F_{1u} + 2A_{2u} + 2E_u + 2F_{2u}$, only five Raman-active vibrational modes of MgAl_2O_4 , $A_{1g} + E_g + 3F_{2g}$, are expected.³⁰ In this study, the spinel phase begins to appear after the sample was heated at 600 °C, and the new Raman peaks became more intense with increasing temperature. After the calcination at 1400 °C, five peaks at 308, 407, 671, 723 and 767 cm^{-1} were observed, which correspond to the five Raman modes $3F_{2g}$, E_g and A_{1g} .

As calcination temperature increased, the XRD peaks became sharper and more intense, indicating that the particles grew in calcinations. The sample particles grow slowly from 6 nm to 12 nm after calcinations below 1000 °C, but grow dramatically faster above 1000 °C (see Fig. 3). As shown in Fig. 2, the characteristic Raman modes of the starting materials at 554 and 1053 cm^{-1} are seen at calcination temperatures up to 1000 °C. The presence of MgAl_2O_4 precursor reactants implies that the resulted MgAl_2O_4 nanoparticles are dispersed in the remaining MgAl_2O_4 precursor reactants, and the particle growth is thus inhibited. Above 1000 °C, no Raman modes of the MgAl_2O_4 precursor were observed, which indicates that the reaction has completed, resulting in direct spinel–spinel nanoparticle contact.

As shown in Fig. 3 and 4, below 1000 °C the change of grain size after each calcination is smaller than the

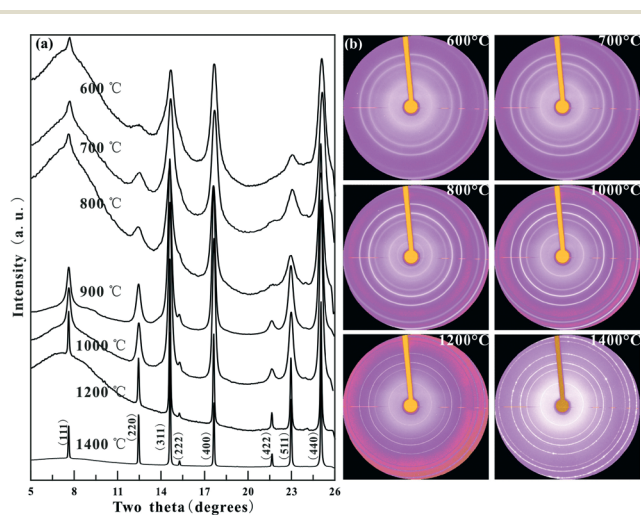


Fig. 1 (a) XRD patterns of the synthesized MgAl_2O_4 crystalline powders calcined at various temperatures. (b) The measured X-ray diffraction images of the MgAl_2O_4 powders.

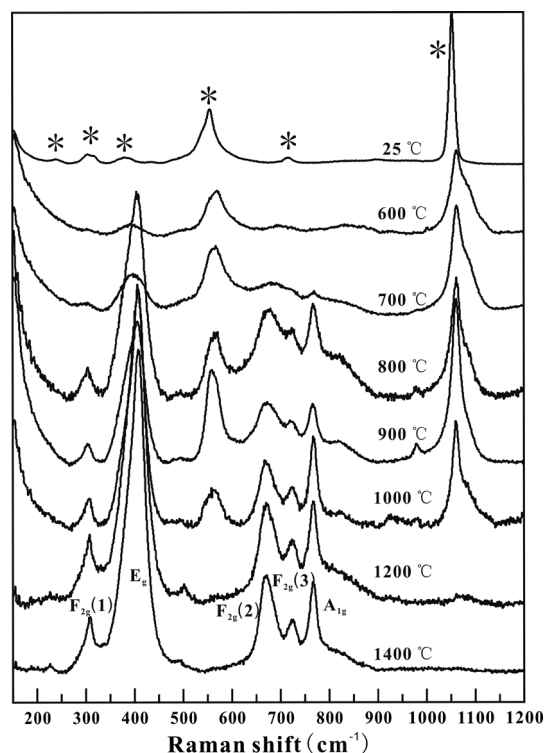


Fig. 2 Raman spectra of the hydroxide precursors of MgAl_2O_4 and postcalcined MgAl_2O_4 powders. Compared with the Raman modes of the hydroxide layer modes of the hydrotalcite,³³ the strong Raman peaks around 1053 cm^{-1} and 554 cm^{-1} (marked with asterisks) can be assigned to the modes of $E_{g(R)}$ (OH) and $E_{g(T)}$ (Mg/Al-OH), respectively. Other weak modes cannot be well identified, possibly coming from the intermediate structures after initial reaction.

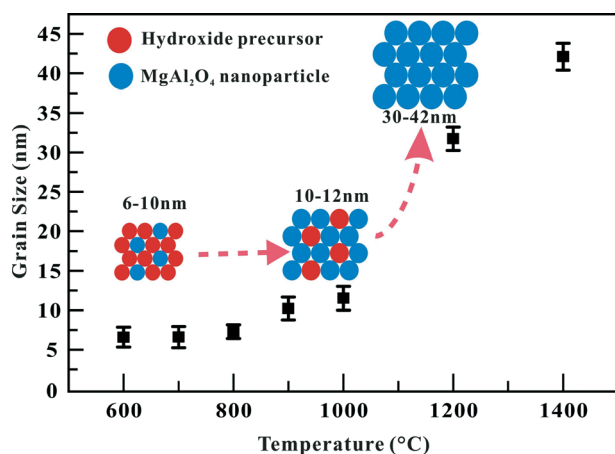


Fig. 3 The average grain size of the MgAl_2O_4 spinel powders as a function of calcination temperature. Two stages of crystal growth can be seen for calcination temperatures below and above $1000\text{ }^\circ\text{C}$.

pre-calcination grain size. Due to mixing of the unreacted hydroxide precursors and the formed spinel nanoparticles, the probability of the direct oriented attachment of the nanoparticles is low. After the calcinations at $1200\text{ }^\circ\text{C}$, the grain size changes by multiple folds. This may result from the grain growth *via* oriented attachment upon consumption

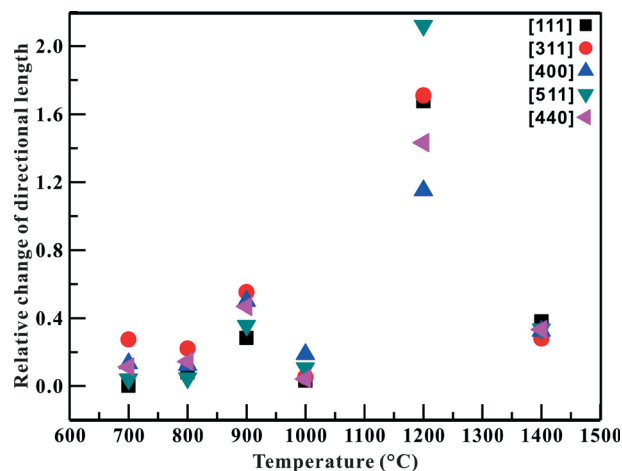


Fig. 4 The relative change of directional length of the MgAl_2O_4 sample with increasing calcination temperature. The relative length change $[(D_{\text{postcalcination}} - D_{\text{precalcination}})/D_{\text{precalcination}}]$ is the fractional length change of the sample in each calcination. The directional length is calculated (using the Scherrer equation³⁴) from the X-ray diffraction peaks (111), (311), (400), (511) and (440).

of the entire precursor matrix. Several studies^{31,32} have demonstrated that nanocrystals can grow by the alignment and coalescence of neighboring particles. The grain boundaries are eliminated in that process. As shown in Fig. 4, the directional length change along [400] is about 118% and about 220% along [511], which suggests that the particle growth *via* oriented attachment is not isotropic. Interestingly, after calcinations at $1400\text{ }^\circ\text{C}$, the relative changes of grain size drop to below 100%. This indicates that oriented attachment is less likely to occur in the calcinations at $1400\text{ }^\circ\text{C}$. The possible reason is that the particles are too large to rotate for the direct oriented attachment.

As shown in Fig. 3, the average grain size stays almost the same after calcinations below $800\text{ }^\circ\text{C}$, suggesting the nanoparticles are fully dispersed in the precursor matrix. The nanocrystals grow somewhat after calcinations at 900 and $1000\text{ }^\circ\text{C}$. Partial aggregation may occur in the calcinations, however, the small grain size change suggests that the grains grow possibly *via* diffusion mechanisms, in which the larger particles grow at the expense of small particles, rather than oriented attachment, where nanoparticles with common crystallographic orientations directly combine together to form larger ones. This observation could be useful in materials synthesis. By introducing intergrain impurities, grain size can be well controlled in nanomaterials synthesis with coprecipitation methods. Fig. 5 shows the relative intensity change of diffraction peaks in the thermally-induced grain growth. The intensity of some peaks increases faster than that of others. We interpret the latter large grain change as a consequence of the nanoparticle elongation due to oriented attachment along a specific direction.

Based on the analysis above, the grain growth of MgAl_2O_4 involves two mechanisms, diffusion and oriented attachment. In the low temperature calcinations ($600\text{--}1000\text{ }^\circ\text{C}$), the

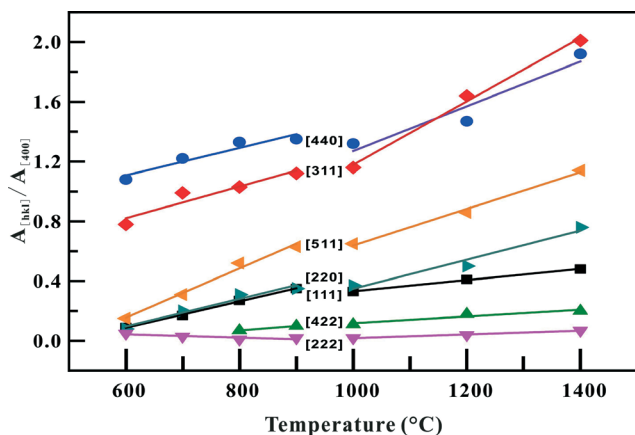


Fig. 5 Relative change of the integrated intensity of different diffraction peaks as a function of calcination temperature.

hydroxide precursor of MgAl_2O_4 and ultrafine nanoparticles (6–12 nm) co-exist. The nucleation center is the hydroxide precursor of MgAl_2O_4 . Because the activation energy for the MgAl_2O_4 nanoparticle growth during the diffusion ripening is higher than that for the phase transformation of hydroxide precursor to nanoparticle, the transformation of hydroxide precursor to nanoparticle is dominant, and the ripening of formed nanoparticles is not onset. After the higher temperature calcinations (1200 °C), the hydroxide precursor MgAl_2O_4 has been transformed completely. The resulted MgAl_2O_4 nanoparticles can aggregate and then the oriented attachment growing mechanism becomes operative. However, calcination at higher temperature (~1400 °C) results in large grains that may disfavor oriented attachment.

Conclusion

The growth of ultrafine MgAl_2O_4 nanocrystals calcined at 600–1400 °C has been examined with Raman and X-ray diffraction techniques. Two growth stages were observed. After calcinations at temperatures below 1000 °C, the coprecipitated hydroxide precursor greatly inhibited the crystallite growth. It is believed that in the post-nucleation stage, crystal growth is realized through diffusion. In the further calcinations above a certain temperature, the hydroxide precursors were used up, and oriented attachment becomes operative till the resulted large crystals cannot rotate enough to facilitate oriented attachment. Grain growth *via* oriented attachment remains under-investigated for the processes of solid solution reaction. For further exploration on this topic, next we would examine the crystal growth in smaller steps of calcination temperature and time. TEM measurements are also planned.

Acknowledgements

We thank the beamline scientists of BL15U1 of the Shanghai Synchrotron Radiation Facility (SSRF) for the technical help. Some preliminary XRD measurements were made at BL12.2.2

of ALS, Lawrence Berkeley National Lab, USA. ALS is supported by the Director, Office of Science, Office of Basic Energy Sciences, of the U.S. Department of Energy (DOE) under contract DE-AC02-05CH11231. We also thank the referees for help with improving the manuscript. Financial support for this study was provided by National Natural Science Foundation of China (41372047, 41272058 and 11179030). This is contribution No. IS-1791 from GIGCAS.

References

- 1 R. L. Penn and J. F. Banfield, *Science*, 1998, **281**, 969–971.
- 2 H. Zhang, M. Finnegan and J. F. Banfield, *Nano Lett.*, 2001, **1**, 81–85.
- 3 R. L. Penn and J. F. Banfield, *Geochim. Cosmochim. Acta*, 1999, **63**, 1549–1557.
- 4 J. F. Banfield, S. A. Welch, H. Zhang, T. T. Ebert and R. L. Penn, *Science*, 2000, **289**, 751–754.
- 5 D. Li, M. H. Nielsen, J. R. Lee, C. Frandsen, J. F. Banfield and J. J. De Yoreo, *Science*, 2012, **336**, 1014–1018.
- 6 D. C. Harris, History of development of polycrystalline optical spinel in the U.S., *Proc. SPIE*, June 22, 2005, vol. 5786, Window and Dome Technologies and Materials IX, 1.
- 7 J. L. Sepulveda, R. O. Loutfy, S. Chang and S. Ibrahim, High-performance spinel ceramics for IR windows and domes, *Proc. SPIE*, May 20, 2011, vol. 8016, Window and Dome Technologies and Materials XII, 801604.
- 8 R. Dal Maschio, B. Fabbri and C. Fiori, *Ind. Ceram.*, 1988, **8**, 121–126.
- 9 L. Rooi Ping, A.-M. Azad and T. Wan Dung, *Mater. Res. Bull.*, 2001, **36**, 1417–1430.
- 10 B. W. Evans and B. R. Frost, *Geochim. Cosmochim. Acta*, 1975, **39**, 959–972.
- 11 P. Burnley and H. Green, *Nature*, 1989, **338**, 753–756.
- 12 H. Green II and P. Burnley, *Nature*, 1989, **341**, 733–737.
- 13 F. Meyer, R. Hempelmann, S. Mathur and M. Veith, *J. Mater. Chem.*, 1999, **9**, 1755–1763.
- 14 M. K. Naskar and M. Chatterjee, *J. Am. Ceram. Soc.*, 2005, **88**, 38–44.
- 15 L. Torkian, M. M. Amini and Z. Bahrami, *J. Inorg. Mater.*, 2011, **26**, 550–554.
- 16 K. Prabhakaran, D. S. Patil, R. Dayal, N. M. Gokhale and S. C. Sharma, *Mater. Res. Bull.*, 2009, **44**, 613–618.
- 17 C. Augustin and R. K. Selvan, *Bull. Electrochem.*, 2003, **19**, 319–334.
- 18 Y. Ding, G. Zhang, H. Wu, B. Hai, L. Wang and Y. Qian, *Chem. Mater.*, 2001, **13**, 435–440.
- 19 Z. Liu, W.-L. Wang, X. Liu, M. Wu, D. Li and Z. Zeng, *J. Solid State Chem.*, 2004, **177**, 1585–1591.
- 20 C. Păcurariu, I. Lazău, Z. Ecsedi, R. Lazău, P. Barvinschi and G. Mărginean, *J. Eur. Ceram. Soc.*, 2007, **27**, 707–710.
- 21 P.-Y. Lee, H. Suematsu, T. Yano and K. Yatsui, *J. Nanopart. Res.*, 2006, **8**, 911–917.
- 22 B. Alinejad, H. Sarpoolaky, A. Beitollahi, A. Saberi and S. Afshar, *Mater. Res. Bull.*, 2008, **43**, 1188–1194.
- 23 N. Khalil, M. Hassan, E. Ewais and F. Saleh, *J. Alloys Compd.*, 2010, **496**, 600–607.

- 24 M. Rashad, Z. Zaki and H. El-Shall, *J. Mater. Sci.*, 2009, **44**, 2992–2998.
- 25 J.-G. Li, T. Ikegami, J.-H. Lee, T. Mori and Y. Yajima, *J. Eur. Ceram. Soc.*, 2001, **21**, 139–148.
- 26 C. R. Bickmore, K. F. Waldner, D. R. Treadwell and R. M. Laine, *J. Am. Ceram. Soc.*, 1996, **79**, 1419–1423.
- 27 J. McHale, A. Navrotsky and R. Kirkpatrick, *Chem. Mater.*, 1998, **10**, 1083–1090.
- 28 J. Rufner, D. Anderson, K. Benthem and R. H. Castro, *J. Am. Ceram. Soc.*, 2013, **96**, 2077–2085.
- 29 A. A. Gribb and J. F. Banfield, *Am. Mineral.*, 1997, **82**, 717–728.
- 30 N. V. Hung and V. X. Quang, *Commun. Phys.*, 2003, **13**, 118–123.
- 31 C. Ribeiro, E. J. H. Lee, T. R. Giraldo, R. Aguiar, E. Longo and E. R. Leite, *J. Appl. Phys.*, 2005, **97**, 1–4.
- 32 A. P. Alivisatos, *Science*, 2000, **289**, 736–737.
- 33 S. J. Palmer, R. L. Frost and T. Nguyen, *Coord. Chem. Rev.*, 2009, **253**, 250–267.
- 34 A. L. Patterson, *Phys. Rev.*, 1939, **56**, 978–982.